AUT Journal of Electrical Engineering
10.22060/EEJ.2026.26087.6057

Design and Control of Quadvoltlift Boost Converter for PV Driven Electric Vehicle System

Arun Kumar Ravindran [1*], Vidhya Chellappa [2], Mutharasu Selvaraj[3], Govinthasamy Nathipalayam Ramasamy [4]

[1]Assistant Professor, Department of Electrical and Electronics Engineering, V.S.B. Engineering College, Karur, Tamil Nadu, India- 639111.

[2]Assistant professor, Department of Electrical and Electronics Engineering, Unnamalai Institute of Technology, Kovilpatti, Tamil Nadu, India- 628502.

[3]Assistant Professor, Department of Electrical and Electronics Engineering, Erode Sengunthar Engineering College, Perundurai, Tamil Nadu, India- 638057.

[4]Assistant Professor (Sl.Gr.), Department of Electrical and Electronics Engineering, Dr. N.G.P. Institute of Technology, Coimbatore, Tamil Nadu, India- 641048.

*Corresponding E-mail: [1]arunrkumar9330@gmail.com

Uncorrected Proof

Abstract:

The incorporation of Renewable energy sources (RES) with Electric vehicle (EV) systems has accelerated owing to the growing demand of environmental friendly transportation. To attain effective power conversion and enhanced system performance, this research develops a QuadVoltLift Boost Converter (QVLB) for EV applications. The QVLB converter is employed to boost the power voltage level with high voltage gain, less switching stress, increased efficiency and fewer components than traditional converters. A Blue Monkey Optimization-based PI (BMO-PI) controller is exploited for the tuning its parameters to guarantee efficient regulation of the DC-link voltage under changing irradiation and load conditions. The optimized controller increases voltage stability, reduces steady-state error and improves dynamic response. A three-phase Voltage Source Inverter (VSI), powers a Brushless DC (BLDC) motor for vehicle propulsion. Additionally, by permitting charging and discharging operations in accordance with system requirements, a battery system interfaced via a bidirectional converter for effective energy management. By efficiently coordinating power flow amide the PV source, battery and traction drive, the developed system rises the overall dependability and efficiency of the system. The simulation outcomes in MATLAB show better

transient performance under different operating situations, superior voltage regulation with efficiency of 94.9 %, signifying the efficiency of QVLB converter for renewable energy based EV system.

Keywords:

EV, PV system, QVLB converter, BMO-PI controller, BLDC motor.

1. Introduction

To ensure a sustainable future, challenges comprising greenhouse gas emissions, diminishing fossil fuel sources and global warming necessitate immediate response [1]. Since the transportation industry is one of the main reasons of the growing hazardous emissions, electrifying transportation is a potential way to address this issue [2]. The technology for EVs are present for more than a century, reaching its commercial peak around 1900 [3]. The advantages that EVs offer in terms of the environment, economy and society make their use vital to the design of modern transportation [4]. Cities and nations develop more ecologically friendly and effective transport systems with the aid of EV laws, infrastructural upgrades and technological developments [5]. Nevertheless, the employment of the concept necessitates massive electrical energy and infrastructure for charging [6]. Additionally, EVs are only sustainable if the power needed for charging from sustainable and RES [7]. Nevertheless, using fossil fuels to produce energy only shifts emissions from vehicle to power plants rather than lowering them [8]. As an outcome, using RES to generate power totally eliminate emissions and assist the environment [9].

PV has a lot of interest among other RES owing to its abundance, scalability and falling technical costs [10, 11]. As PV module prices continue to decline, solar power is becoming more widely acknowledged as a competitive energy source to complement the grid [12]. PV-based systems have intrinsic restrictions when used directly for EV charging applications. PV modules provide a low, erratic direct current voltage that is highly dependent on temperature and irradiation [13]. The DC/DC converter is vital in PV system for overcoming the difficulties caused by the environmental variations. The Transformer-Less Quadratic

Uncorrected Proof

10.22060/EEJ.2026.26087.6057

Buck-Boost [14] Converter increases power density while decreasing size, weight and cost. It delivers comparatively easy control and uninterrupted power transfer. Nevertheless, at high conversion ratios, semiconductor devices experience high voltage stress. An isolation transformer is not necessary for the Non-Isolated High-Gain Quadratic Boost [15] Converter to obtain extremely high voltage gain. The complexity and cost of the circuit rise with the active and passive components count. The Switched Inductor–Capacitor [16] Converter delivers superior energy transfer capabilities and is suitable for low-input-voltage applications. The size and complexity of the circuit are raised by adding more switches, capacitors and inductors.

The Active Switched-Inductor Network Step-Up [17] Converter rises efficiency and dynamic performance. Control complexity and gate-driving requirements are improved when additional active switches are required. By attaining a quadratic voltage gain, the Non-Isolated Quadratic High-Gain [18] Converter permits high output voltages from low input sources without the need for magnetic isolation. Cumulative losses in numerous energy-transfer stages cause efficiency to drop, particularly when there is a high load. Although high gain [19] converters attain very large voltage conversion ratios in a single stage, they have issues like improved conduction and switching losses, high semiconductor voltage stress and decreased efficiency at severe duty cycles. The voltage step-up capability of the improved high gain [20] converter with cascaded boost stages is greatly increased without sacrificing efficiency. If the converter is not correctly optimised for high gain operation, it also experience improved switching losses and voltage stress across semiconductor devices. Thus, the QVLB converter is developed in this research for raising the PV voltage in the EV applications.

The PI controller is utilized to manage the PV voltage and its parameters are tuned by the metaheuristic algorithm. Strong global search capabilities, quick convergence and a good capacity to break out from local optima through producer-scrounger behaviour characterise the Sparrow Search Algorithm (SSA) [21]. Since, the SSA experiences population variety loss in subsequent iterations and premature convergence in

Uncorrected Proof

complicated multimodal issues. Crow Search Optimisation (CSA) [22] is adaptable and appropriate for nonlinear optimisation issues. The selection of awareness probability determines the quality of the solution. To get consistent results, it take several runs. The Lion Grey Wolf Optimisation [23] Algorithm works well for both preserving population variety and resolving challenging optimisation issues. Optimisation performance and convergence speed are negatively impacted by indecorous parameter fine-tuning. The dragonfly algorithm's capability to evade local optima is improved by the Chaotic Dragonfly Optimisation [24], which also rises population diversity. Owing to the chaotic map integration and optimisation processes, the algorithm has a greater computational complexity. Henceforth, the above difficulties are solved by the utilization of BMO-PI controller with better regulation of PV voltage. The main contributions are,

- To attain better voltage gain without requiring an excessive duty cycle, the QuadVoltLift Boost Converter raises the voltage output with superior voltage gain.
- By managing the QVLB converter output voltage under various solar irradiation and load situations, the BMO-PI controller enhances dynamic response, lowers overshoot and diminishes steady-state error.
- The incorporation of battery provides power during periods of poor solar availability or unpredicted load demands by stowing excess PV energy during periods of excess generation.

2. Proposed System Description

The solar energy is transformed into power by a PV array as the main renewable energy source. The PV array's output voltage is changeable and contingent based on temperature and irradiation. A QuadVoltLift boost converter receives the PV output to rise the DC voltage. A steady DC bus voltage is regulated with the aid of a Blue Monkey PI controller. Subsequently, a PWM generator that generates switching pulses for the QuadVoltLift boost converter. To guarantee dependable operation during power fluctuations, a

Uncorrected Proof

10.22060/EEJ.2026.26087.6057

bidirectional converter integrates a battery energy storage system to store the excess energy from the PV system. A PI controller generates the reference battery current by processing the inaccuracy that results from comparing the battery voltage with the reference battery voltage. The current error signal is then obtained by comparing the reference current with the actual battery current. The bidirectional converter is managed by a PWM generator using the output of a second PI controller that receives this current error. The bidirectional converter either uses excess PV power to charge the battery or empties the battery to support the DC bus when solar generation is insufficient, depending on the operating conditions. The block diagram for PV based EV system is presented in Fig. 1.

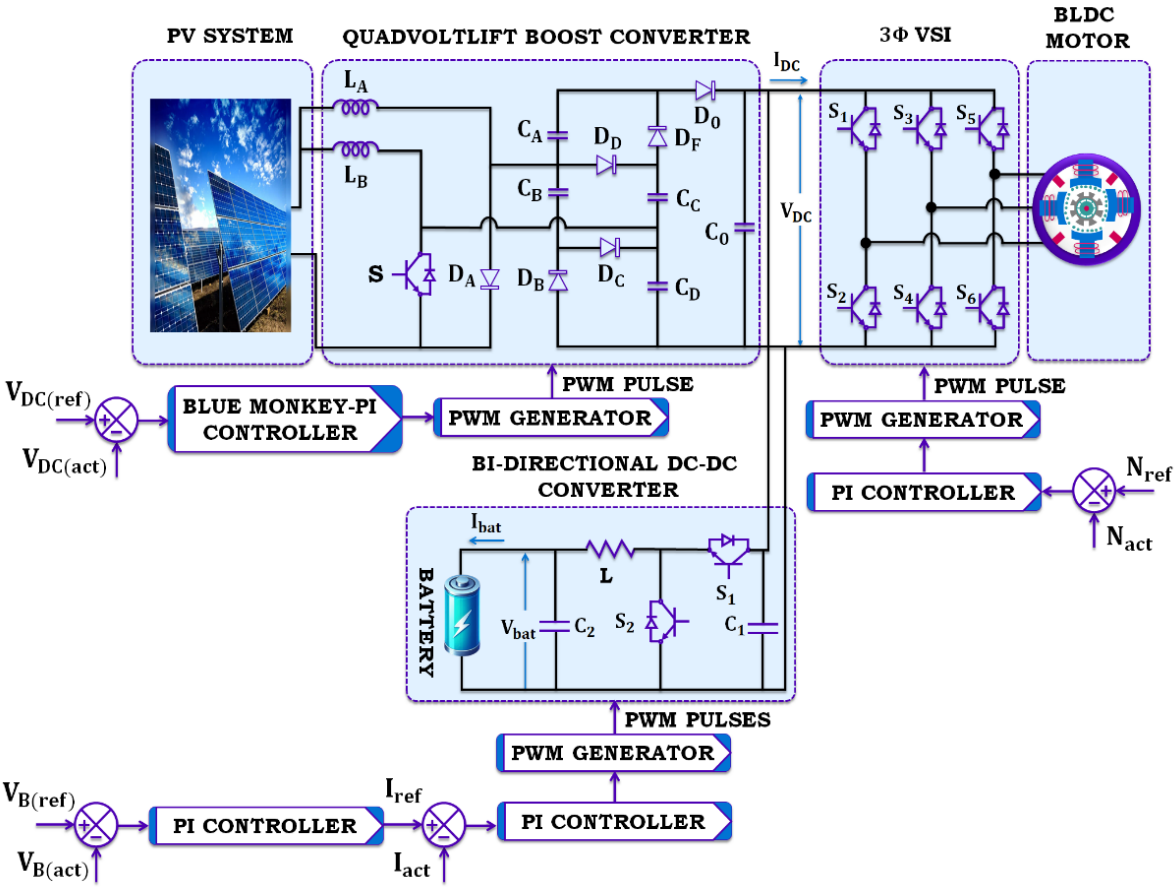


Fig. 1. Block diagram of PV based EV system

For motor drive applications, VSI receives the DC bus voltage. A PI controller is employed to process the speed error after motor speed reference and actual motor speed are compared. A PWM generator transforms

10.22060/EEJ.2026.26087.6057

the controller output into switching signals, which control the three-phase VSI's functioning. The DC bus voltage is transformed by the VSI into the regulated three-phase AC power that the BLDC motor requirements. Thus, for high-performance and electric mobility applications, the QuadVoltLift Boost Converter with BMO-PI control provides an efficient solution.

2-1- PV System

The sunlight is transformed into electrical energy by PV cells, which are semiconductor devices. The strength of the temperature, light and the fundamental characteristics of the cell material all impact a solar cell's efficiency. The one diode model is normally utilized and its circuit is represented in Fig. 2. The current characteristics is,

$$I_{ph} - I_o\left[e^{q\frac{(V_{PV}+R_S I_{PV})}{AkT_j}} - 1\right] = \frac{V_{PV}}{R_{sh}} \quad (1)$$

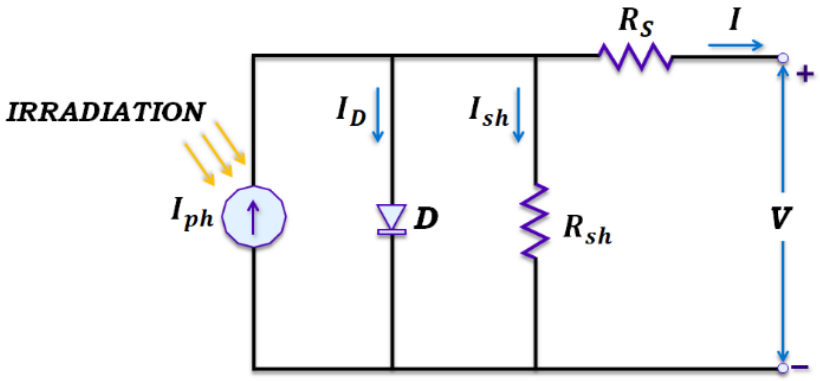


Fig. 2. Circuit of PV system

Here, the junction temperature is T, the photocurrent is I_{ph}, output voltage is V_{PV}, charge on an electron is q, ideality factor is A, shunt resistance is R_S, diode saturation current is I_o and series resistance is R_S. Nevertheless, the low PV voltage is caused owing to the ecological variations and is effectively enhanced by the QVLB Converter and its function is described below.

Unedited Proof

10.22060/EEJ.2026.26087.6057

2-2- QVLB Converter

The QVLB Converter is developed to provide a far greater voltage conversion ratio than the boost converter. The converter employs a voltage-lift network made up of many diodes and capacitors that store and transfer energy. Two inductors (L_A, L_B), five capacitors$(C_A, C_B, C_C, C_D \; and \; C_O)$ one switch (S) and six diodes $(D_A, D_B, D_C, D_D, D_E) \; and \; D_O$, develops the converter, as depicted in Fig. 3.

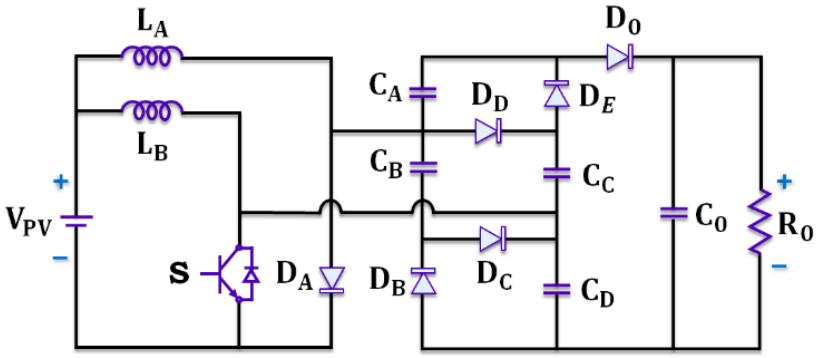


Fig. 3. Circuit of QVLB Converter

It is appropriate for PV system since it enhances efficiency, lowers voltage stress across the semiconductor devices and enhances voltage gain. To generate a high output voltage, the QVLB employs two switching modes in which the inductors are charged during the switch ON stage and release their stowed energy via the voltage-lift cells during the switch OFF stage. The waveform of QVLB Converter is depicted in Fig. 4. When compared to traditional converters, the QVLB converter's two inductors, five capacitors, and six diodes rise component cost, circuit complexity and PCB space even though it delivers high voltage gain with less semiconductor voltage stress. On the other hand, the high voltage gain make it unnecessary to use additional cascaded conversion stages, which result in a smaller and less expensive system. In EV applications, weight and packaging requirements are crucial factors that is improved by the employment of numerous passive components.

Uncorrected Proof

10.22060/EEJ.2026.26087.6057

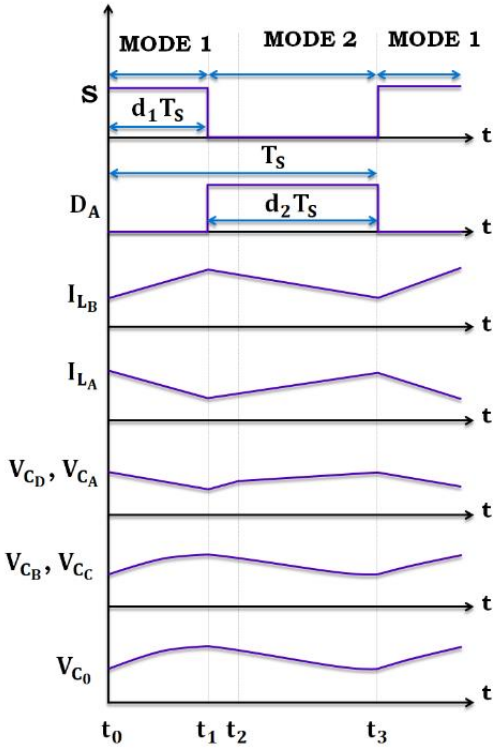


Fig. 4. Waveform of QVLB Converter

Mode 1:

In stage1, S is activated, developing a low-resistance path that enables $L_A$and L_B to energised by V_{PV}. As a result, both inductors store energy and have linearly increasing currents. While D_C, D_D and D_O become active and conduct, D_A, D_B and D_E are inactive and prevent current flow via their branches, as displayed in Fig. 5 (a). In accordance with the converter, the conducting diodes enable $C_A, C_B\ C_C\ and\ C_D$to be charged. Consequently, the capacitor C_O simultaneously provides energy to the load. Applying KVL,

$$V_{L_B} = V_{PV} \tag{2}$$

$$V_{C_C} = V_{C_A} + V_{C_B} \tag{3}$$

$$V_{C_A} = V_{C_B} = V_{PV} \tag{4}$$

$$V_{C_C} = 2V_{PV} \tag{5}$$

Uncorrected proof

10.22060/EEJ.2026.26087.6057

$$V_{C_D} = V_{C_B} = V_{PV} \tag{6}$$

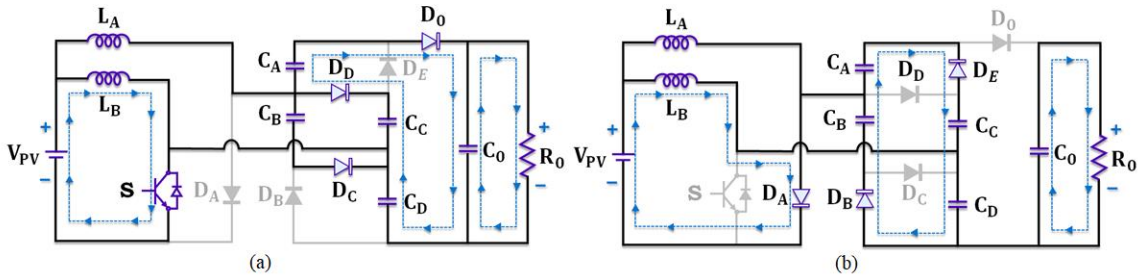


Fig. 5. Modes of QVLB Converter (a) Mode 1 (b) Mode 2

Mode 2:

The stowed energy in the inductors$L_A$and L_B must be released to the output stage when S is turned off during Mode 2, as revealed in Fig. 5(b). D_A, D_B and D_E become forward-biased and offer conduction paths for the discharge currents when the inductor voltages reverse polarity. Simultaneously, D_C, D_D and D_O are inactivated and prevent current from passing through their branches. By connecting the input source and the discharging inductors in series with $C_A, C_B\ C_C\ and\ C_D$, the voltage delivered to the output side is increased. Thus, the load and the C_O are both charged. Applying KVL,

$$V_{L_B} = V_{PV} - V_{C_B} \tag{7}$$

$$V_{L_B} = 0 \tag{8}$$

Apply volt-second balance law,

$$V_{PV} D + (1-D)\left(V_{PV} - V_{C_B}\right) = 0 \tag{9}$$

$$V_{C_B} = \frac{V_{PV}}{1-D} \tag{10}$$

$$V_{C_A} = \frac{V_{PV}}{1-D} \tag{11}$$

$$V_{C_C} = V_{C_A} + V_{C_B} = \frac{2V_{PV}}{1-D} \tag{12}$$

Uncorrected Proof

10.22060/EEJ.2026.26087.6057

$$V_{C_D} = \frac{V_{PV}}{1-D} \tag{13}$$

$$V_O = V_{PV} + V_{C_A} + V_{C_B} + V_{C_C} + V_{C_D} \tag{14}$$

$$V_O = V_{PV} + \frac{V_{PV}}{1-D} + \frac{V_{PV}}{1-D} + \frac{2V_{PV}}{1-D} + \frac{2V_{PV}}{1-D} \tag{15}$$

$$V_O = V_{PV} + \frac{5V_{PV}}{1-D} \tag{16}$$

The voltage gain is,

$$\frac{V_O}{V_{PV}} = \frac{6-D}{1-D} \tag{17}$$

The voltage stress on switch is,

$$V_s = \frac{V_{PV}}{1-D} \tag{18}$$

With lower switching losses and higher energy conversion efficiency, the QVLB effectively produces an enhanced voltage. Its minimal component stress and improved voltage gain support dependable system performance. The voltage fluctuations are solved by utilizing Pi controller and its parameters are tuned by BMO algorithm.

2-3- BMO-PI Controller

The BMO algorithm is employed to tune $k_p$and k_i of PI controller to iteratively search for the ideal controller parameters that offer superior dynamic response and decreased steady-state error in fluctuating irradiance and load conditions. Every monkey in the population serves as a candidate solution with two PI controller gains during this optimisation process. The monkeys are first dispersed at random within the predetermined search space of the controller settings and a fitness function is employed to evaluate each candidate solution's performance. The leader monkey corresponds to the present optimal set of PI gains is the monkey with the highest fitness value. The remaining monkeys' positions are then updated in

Uncorrected Proof

10.22060/EEJ.2026.26087.6057

accordance with the social behaviour of blue monkey swarms, where each monkey modifies its approach to the leader by taking into consideration its own strength (rate), the alteration between its weight and the leader's weight and the positional difference between its present solution and the optimal solution. The updating mechanism is,

$$Rate_{i+1} = (0.7 \times Rate_i) + (W_{leader} - W_i) \times rand \times (X_{best} - X_i) \quad (19)$$

$$X_{i+1} = X_i + Rate_{i+1} \times rand \quad (20)$$

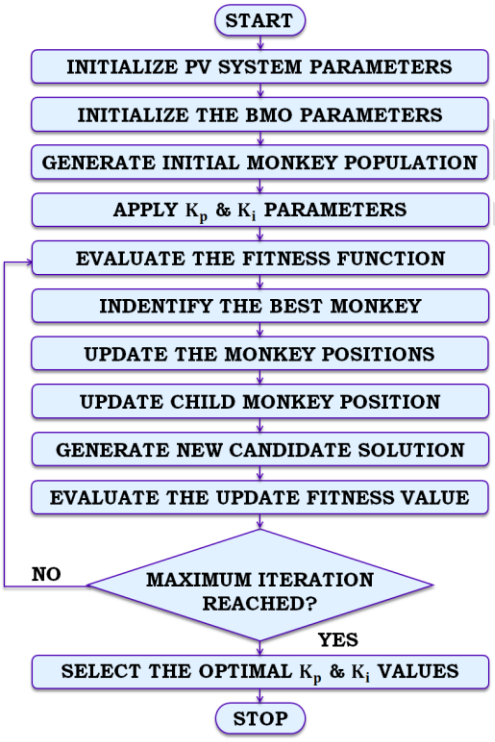


Fig. 6. Flowchart of BMO-PI controller

The flowchart of BMO-PI controller is depicted in Fig. 6. Where, $rand$ is a uniformly distributed random number, W_{leader} and W_i indicate the weights of the leader and the associated monkey and $Rate_i$ signifies the monkey's capability to move. By utilizing this position updating strategy, the search agents gradually approach areas of the solution space that display potential while continuing exploration to avert premature convergence. The young monkeys are also updated that further rise population variety and preserve a balance among exploitation and exploration.

Uncorrected Proof

10.22060/EEJ.2026.26087.6057

$$Rate^{ch(i+1)} = \left(0.7 \times Rate^{ch(i)}\right) + \left(W^{ch(leader)} - W^{ch(i)}\right) \times rand \times X^{ch(best) - X^{ch(i)}} \quad (21)$$

$$X^{ch(i+1)} = Rate^{ch(i+1)} \times rand \quad (22)$$

Where, $W^{ch(leader)}$is the weight of the child leader, $W^{ch(i)}$is the weight of the child monkey, $X^{ch(i)}$is the candidate solution and $X^{ch(best)}$specifies the best child solution. The monkey that yields the lowest fitness value is selected as the new leader after each cycle, while the revised PI gain combinations are reassessed. Until the convergence condition or the maximum iterations count is met, this iterative process is continued. The BMO algorithm's ideal values of $k_p$and $k_i$are then applied to the PI controller, permitting better DC-link voltage regulation, decreased transient fluctuations and stable operation of the EV drive under a variability of operating circumstances. When compared to traditional techniques, the BMO-PI controller significantly reduces steady-state error and increases transient response. Strong voltage regulation is ensured by the optimised gain selection in spite of fluctuations in input and load demand. Thus, the BMO-PI controller increases the EV power system's overall performance. For further improvement in performance, the battery system is employed in this research.

2-4- Battery

The battery is employed for storing the surplus energy generated from the PV system and is employed while the power from PV system is low. System dependability and operational flexibility are enhanced by the bidirectional power flow capability. By applying Kirchhoff's law,

$$V_b(t) = V(h(t) - R^{*}i(t) - V_{ca}(t) \quad (23)$$

$$\frac{dV_{ca}(t)}{dt} = -\frac{1}{c_{pi}R_{pi}}V_{ca}(t) + i(t) \quad (24)$$

The voltage across RC is $V_{ca}(t)$,terminal current is $i(t)$ and the terminal voltage is indicated by $V_b(t)$,. By preserving power balance under transitory operation conditions, the battery storage unit efficiently supports energy management. The bidirectional converter's numerous cycles of charging and discharging hasten

Uncorrected Proof

10.22060/EEJ.2026.26087.6057

battery deterioration over time by raising electrode stress, internal resistance and capacity decline. The battery's State of Health (SOH) is lowered by rapid current fluctuations and high operating temperatures, which also accelerate electrochemical ageing. Battery-aware energy management manages battery temperature, maintain appropriate State of Charge (SOC) restrictions and restrict excessive current changes to lessen these consequences.

2-5- BLDC Motor

The BLDC motors have a high roughness, low maintenance and are simple to control. It offers a low working voltage range, quick dynamic responses, high torque and an excellent performance ratio. A permanent magnet stator and three-phase windings in the rotor develop the BLDC motor. Fig. 7 displays the circuit of a BLDC motor. The 3ϕ winding governing equation is,

$$\begin{bmatrix} V_a^* \\ V_b^* \\ V_c^* \end{bmatrix} = R^* \begin{bmatrix} 1 & 0 & 0 \\ 0 & 1 & 0 \\ 0 & 0 & 1 \end{bmatrix} \begin{bmatrix} i_a^* \\ i_b^* \\ i_c^* \end{bmatrix} + \begin{bmatrix} l-m & 0 & 0 \\ 0 & l-m & 0 \\ 0 & 0 & l-m \end{bmatrix} \frac{d}{dt} \begin{bmatrix} i_a^* \\ i_b^* \\ i_c^* \end{bmatrix} + \begin{bmatrix} E_a^* \\ E_b^* \\ E_c^* \end{bmatrix} \tag{25}$$

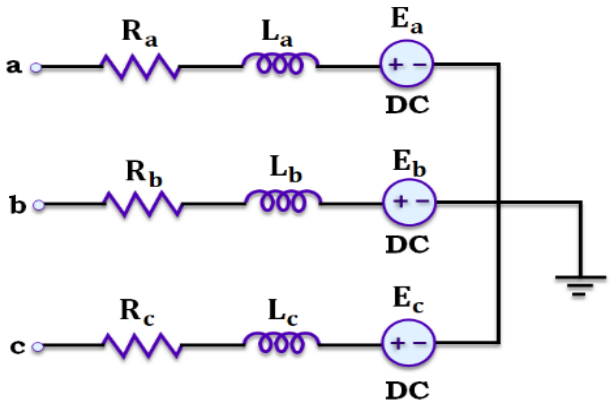


Fig. 7. Circuit of BLDC motor

Here, the mutual inductance is m, phase resistance is R^* and inductance is l.The mechanical equation is,

$$J^* \frac{d\omega_r^*}{dt} = T_e^* - T_l^* - \omega_r^* f_r^* \tag{26}$$

Uncorrected Proof

10.22060/EEJ.2026.26087.6057

Throughout system operation, the BLDC motor demonstrates smooth speed control, effective energy use, and dependable driving performance. Thus, in the renewable energy-based EV system, the BLDC motor guarantees reliable propulsion performance.

3. Result and Discussion

This section analyses an outcomes of PV-EV system in MATLAB tool and its performance is compared over other approaches. The parameters of the developed work is depicted in Table 1.

Table 1. Parameters of the developed work

Parameters	Specification
PV SYSTEM	
Rated power	15 kW
Cells in shunt connection	6
Maximum Peak Current	8.35 A
Voltage (Open circuit)	37.25V
Series attached cells	9
Maximum Peak Voltage	29.95 V
Current (Short circuit)	8.95 A
QVLB CONVERTER	
C_A, C_B, C_C, C_D	22 μF
L_A, L_B	4.7mH
C_O	2200 μF
Switching frequency	10kHz
BATTERY	
Nominal voltage	420 V
Response time	30 s
Initial SOC	80%
Rated capacity	100 Ah
BLDC MOTOR	
Phase resistance	2.3
Phase inductance	7.68e-3
Back EMF flat area	120°
Rotor flux position when theta=0	90° behind A axis

Uncorrected Proof

10.22060/EEJ.2026.26087.6057

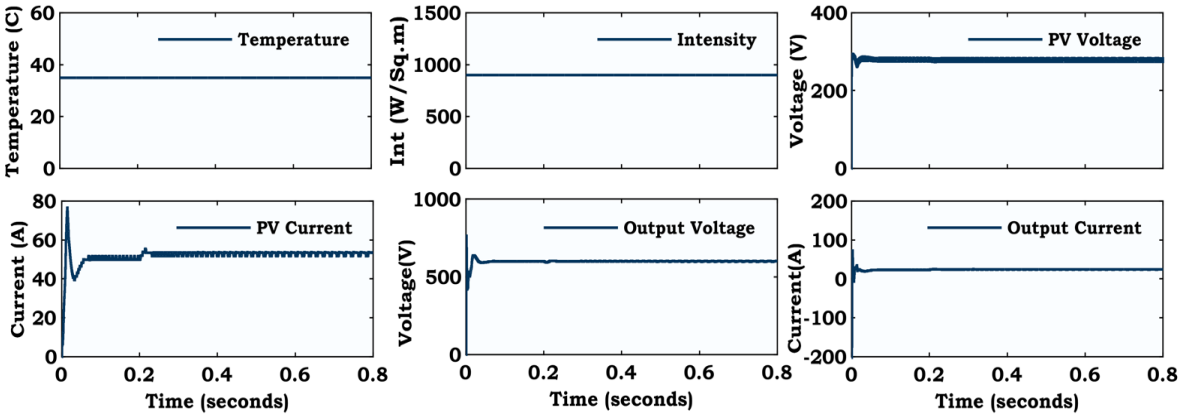


Fig. 8. Waveform of PV system and QVLB converter in constant condition

The temperature and irradiance are sustained at $35°C$ and $900\ W/m^2$, guaranteeing steady conditions, as seen in Fig. 8. Effective voltage enhancement under constant operating conditions is demonstrated by the PV voltage's brief transient response and stabilisation at 298 V. The PV source's effective power extraction is confirmed by the PV current settled at 53 A. The output voltage quickly attains a constant value of 600 V with few oscillations. Consistent and dependable power delivery to the EV load is guaranteed by the output current is stabilised at 25 A.

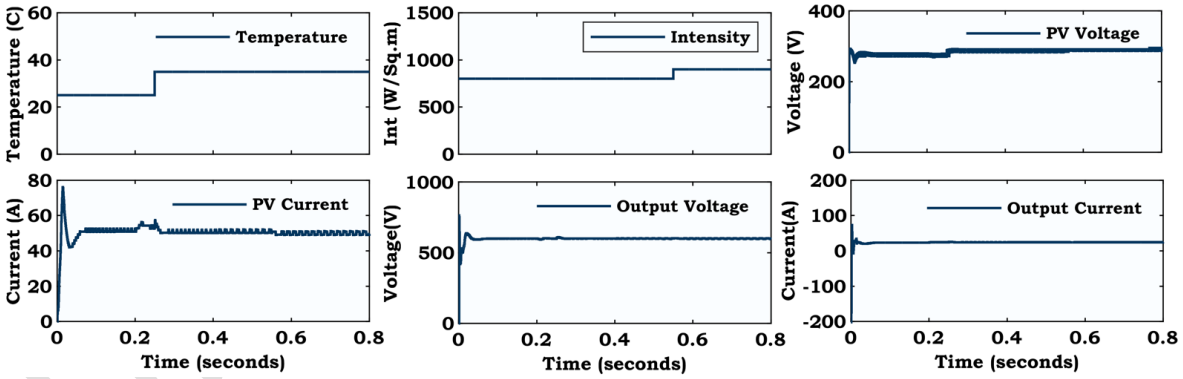


Fig. 9. Waveform of PV system and QVLB converter in varying condition

The waveform of PV system and QVLB converter in varying condition is depicted in Fig. 9. The temperature waveform's step difference and steadying at $35°C$. Furthermore, the irradiance differs stepwise before sustaining at $900\ W/m^2$, which provides a steady supply of solar energy. Effective voltage regulation is confirmed by the PV voltage's smooth response to ecological variations and steady value of

10.22060/EEJ.2026.26087.6057

295 V. Effective power extraction is demonstrated by the PV current, rises with variations in irradiance and stabilises at 50 A. Strong DC-link stability is demonstrated by the output voltage, which is maintained at 600 V. The output current ensures a dependable load supply by following a smooth transient and maintained at 25 A.

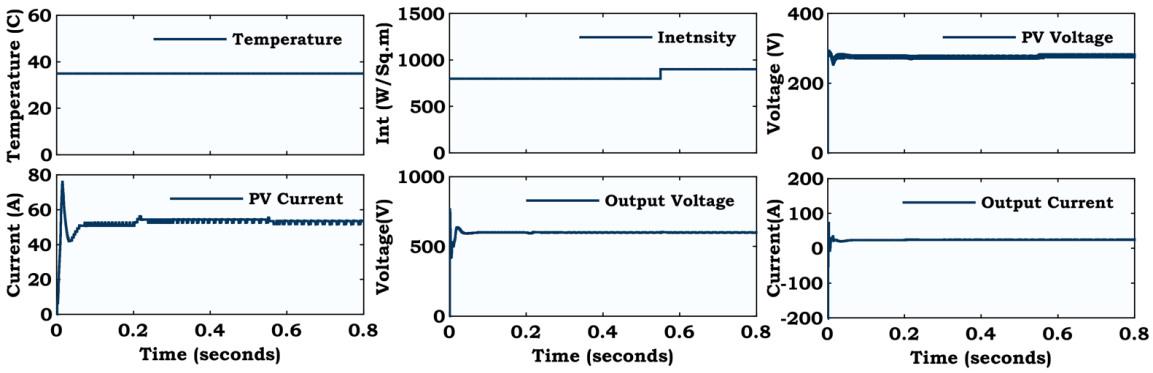


Fig. 10. Waveform of PV system and QVLB converter in constant temperature and varying intensity condition

With a settled value of $35°C$, the temperature stays steady, signifying stable thermal conditions. To ensure sufficient and reliable solar energy input for power generation, the irradiance exhibits a step variation and stabilises at $900\ W/m^2$. Effective voltage improvement is revealed by the PV voltage, which has a quick transient response and settles at 295 V. The PV current confirms effective power extraction from the PV source by responding to variations in irradiance and stabilising at 50 A, as presented in Fig. 10. Robust DC-link voltage regulation is demonstrated by the output voltage's low transient fluctuations and steady value of 600 V. After a brief settling period, the output current stays steady and has a value of 25 A, guaranteeing steady and seamless power delivery to the EV load.

Uncorrected

10.22060/EEJ.2026.26087.6057

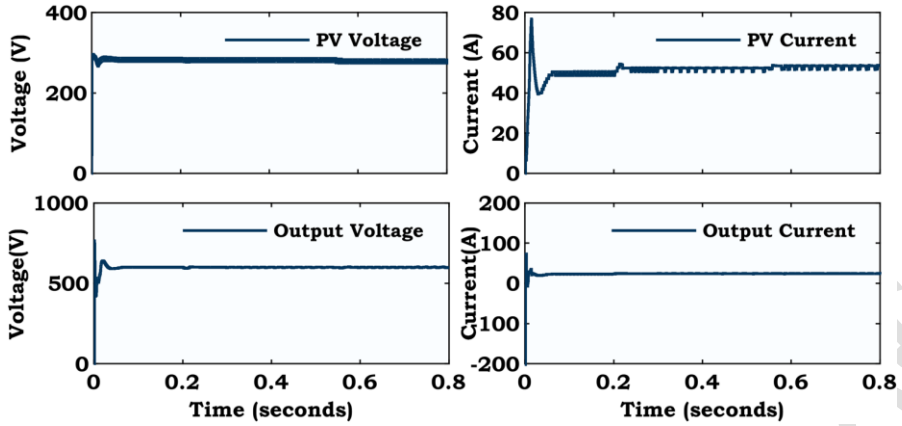


Fig. 11. Waveform of PV system

The PV array voltage quickly stabilises and stays nearly constant at 285 V under partial shade conditions, representing efficient voltage regulation despite the irradiance mismatch. After a brief burst, the PV current settles at 52 Aand shows slight periodic changes. As a result, voltage boosting are demonstrated by the converter output voltage attainment a steady value of 600 V. Stable power transfer from the PV source to the EV drive system is confirmed when the output current stabilises at 25 A with very little ripple, as shown in Fig. 11.

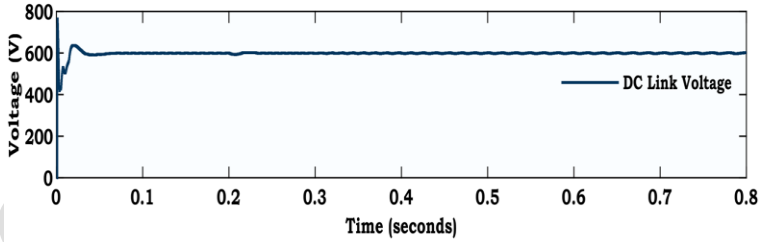


Fig. 12. Waveform of DC-link

Fig. 12 represent the waveform of DC-link and its voltage is sustained at 600 V, representing superior control and adequate energy buffering capacity. The strong controller performance under non-uniform irradiation are specified by the few oscillations.

Uncorrected Proof

10.22060/EEJ.2026.26087.6057

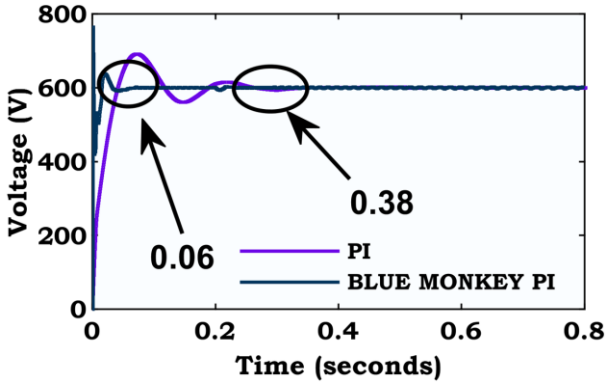


Fig. 13. Waveform of PI and BMO-PI controller

Although having very dissimilar dynamic performances, the DC-link voltage response comparison shows that both controllers are able to manage the voltage to the steady-state value of 600 V. Before settling, the PI controller has a greater overshoot and discernible oscillations; it takes 0.38 seconds to reach steady-state operation. The BMO-PI controller have less overshoot and a earlier settling time of 0.06 seconds, as displayed in Fig. 13.

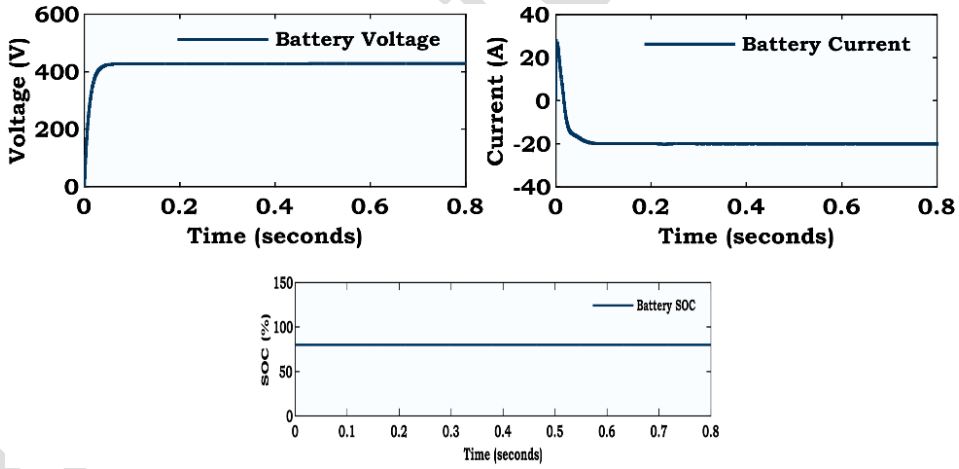


Fig. 14. Waveform of battery

The battery voltage rapidly stabilises at 420 V, presenting reliable energy management in the PV-driven electric vehicle system, as seen in Fig. 14. The battery functions in a charging mode and absorbs excess energy from the PV source while preserving power balance, as seen by the battery current settling at −18

10.22060/EEJ.2026.26087.6057

A. Concurrently, the battery's state of charge (SOC) stays constant at 80%, representing steady battery functioning with little reduction.

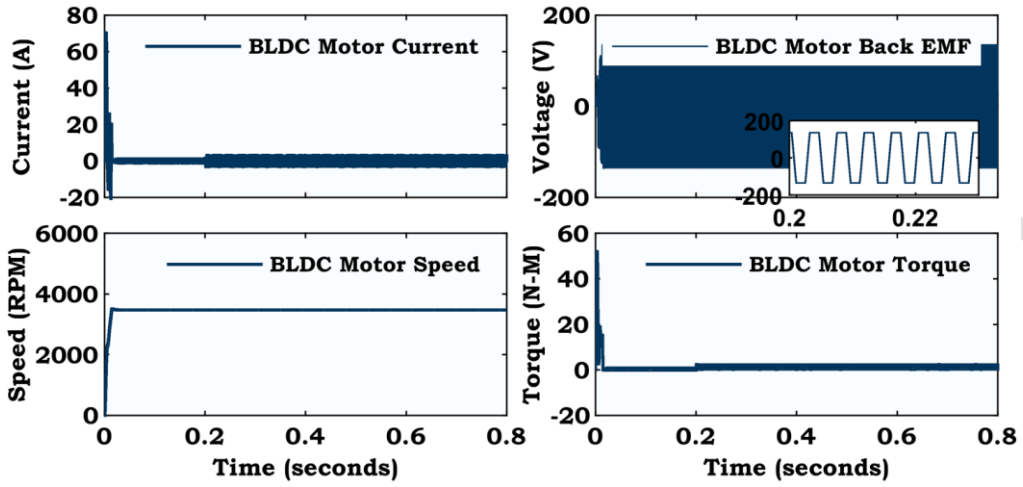


Fig. 15. Waveform of BLDC motor

The waveform of BLDC motor is shown in fig. 15. The back EMF has a constant waveform with a peak value of 150 V, demonstrating good electromagnetic performance, while the BLDC motor current maintains at 2 A. Furthermore, under steady-state working conditions, the torque settles near 2 $N \bullet m$ and the BLDC motor speed stabilises at 3500 RPM, presenting smooth propulsion characteristics and dependable load driving capacity.

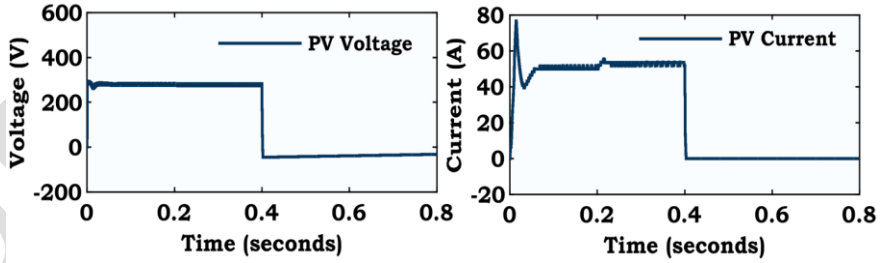


Fig. 16. Waveform of PV system **(**PV disconnected at 0.4s battery powering the BLDC motor)

Uncorrected

10.22060/EEJ.2026.26087.6057

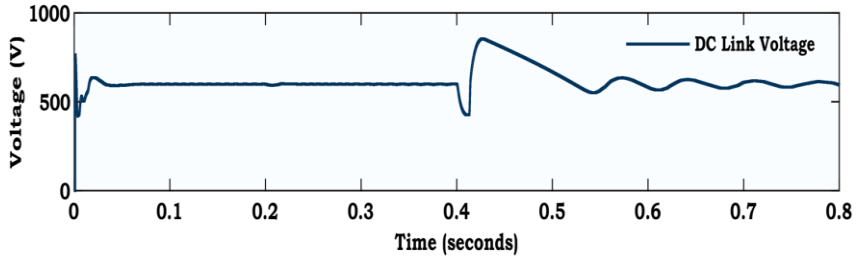


Fig. 17. Waveform of DC link

While the PV current is maintained at 52 A before dropping to 0 A, confirming the loss of PV power contribution after the transition, the PV voltage settles at 280 V and undergoes a sharp reduction at 0.4 s, representing the battery delivers the power to the BLDC motor, as revealed in Fig. 16. The DC-link voltage is steadied at 600 V with more oscillations, as presented in Fig. 17.

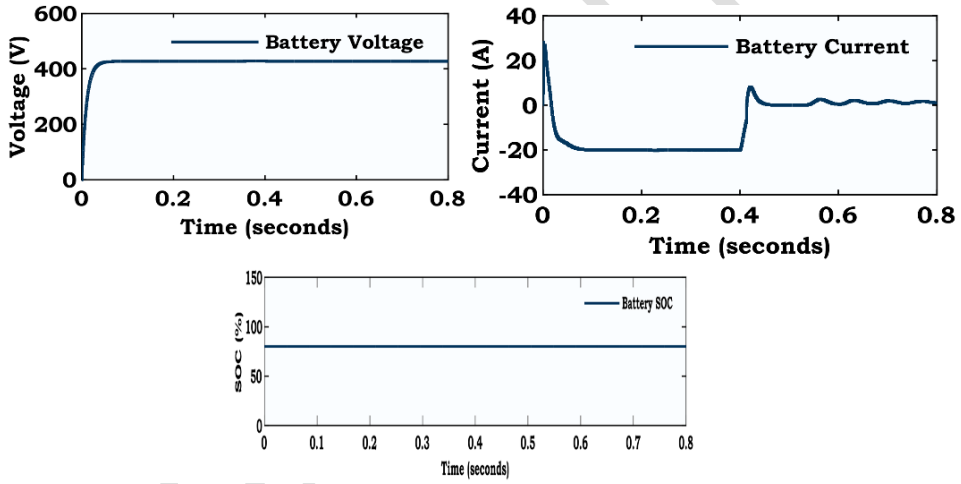


Fig. 18. Waveform of battery

The waveform of battery is revealed in Fig. 18. Effective battery-side voltage regulation is demonstrated when the battery voltage quickly reaches a steady value of 420 V and stays almost constant. After 0.4 seconds, the battery current reverses to 3 A with damped oscillations, signifying that the battery starts providing power to sustain the vehicle load when PV output lowers. Primarily, the current settles at 20 A, indicating battery charging. The SOC stays almost constant at 90% throughout the duration, signifying that the total PV-driven EV system maintains steady and dependable operation.

Uncorrected Proof

10.22060/EEJ.2026.26087.6057

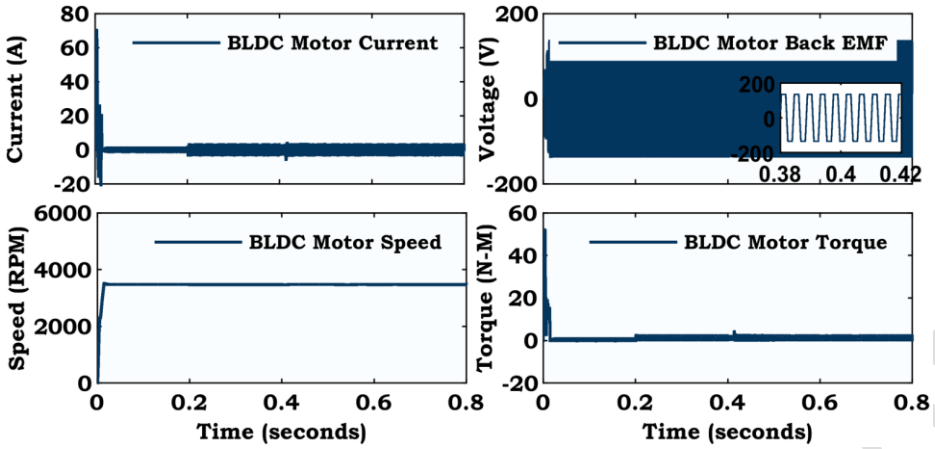


Fig. 19. Waveform of BLDC motor

The waveform of BLDC motor is revealed in Fig. 19. After the transitory period, the BLDC motor current settles at 4 A. Consequently, the BLDC motor back EMF stabilises with a value of 150 V, representing stable electromagnetic energy conversion. Effective speed control and adequate power support from the PV-battery energy system are revealed by the motor speed, which quickly sustains a steady value of 3500 RPM. Subsequently, torque settles at $3\ N \bullet m$ with a slight ripple, which is adequate to meet the load demand.

Table 2. Analysis of voltage gain

CONVERTER	VOLTAGE GAIN	VOLTAGE GAIN AT D=0.6
Transformer-less quadratic buck-boost	$\frac{D}{(1-D)^2}$	3.75
Non-Isolated High Gain Quadratic Boost	$\frac{1+D}{(1-D)^2}$	10
Switched Inductor-Capacitor	$\frac{2-D}{(1-D)^2}$	8.75
Proposed	$\frac{6-D}{1-D}$	13.5

Owing to its fundamental quadratic dependence on duty ratio, the transformer-less quadratic buck-boost [14] converter provides the lowest voltage gain of 3.75 at D=0.6. In contrast, the non-isolated high gain quadratic [15] boost and switched inductor-capacitor [16] converters rise the gain to 10 and 8.75, by enhancing energy transfer via modified inductor-capacitor structures, as shown in Table 2. On the other hand, owing to its linear inverse duty-cycle characteristic and additional gain factor, the QVLB converter

Uncorrected Proof

10.22060/EEJ.2026.26087.6057

attains the highest voltage gain of 13.5, which makes it more suitable for PV-fed and EV systems where high voltage conversion efficiency is needed.

Table 3. Analysis of voltage stress

CONVERTERS	VOLTAGE STRESS	VOLTAGE STRESS AT D=0.6
High gain converter	$\frac{2+36.5D}{5-1.25D}$	5.624
Improved high voltage gain converter with boost stages	$\frac{1}{1-D}$	2.5
Proposed	$\frac{1}{1-D}$	2.5

The high gain [19] converter shows the maximum voltage stress of 5.624 at D=0.6 because of its nonlinear stress dependence on duty ratio, as depicted in Table 3. On the other hand, the enhanced boost-stage [20] converter and the developed converter both function with an inverse duty-cycle relationship, which dramatically lowers voltage stress to 2.5, signifying improved semiconductor stress management and improved suitability for high-efficiency PV and EV applications.

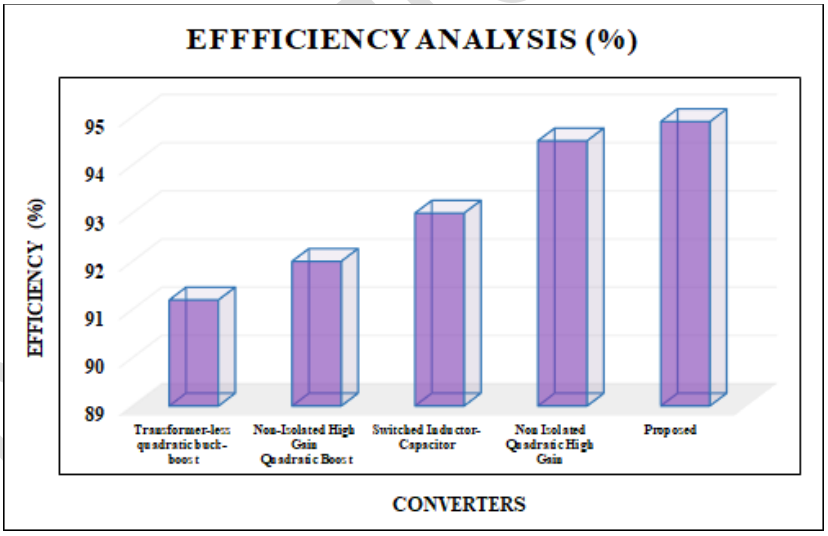


Fig. 20. Analysis of efficiency

According to the efficiency analysis of converters, the high gain quadratic boost [15] converter rises performance to 92%, the transformer less quadratic buck boost [14] converter attains an efficiency of 91.2% and the switched inductor-capacitor [16] converter further rises efficiency to 93% owing to its improved

Unedited Proof

10.22060/EEJ.2026.26087.6057

energy transfer and lower conduction losses, as represented in Fig. 20. In contrast, due to a better voltage gain structure and less switching stress, the non-isolated quadratic high gain [18] converter exhibits a greater efficiency of 94.5%. Because of its optimised switching operation and lower component losses, the QVLB converter achieves the greatest efficiency of 94.9%, presenting enhanced performance under PV-driven EV systems.

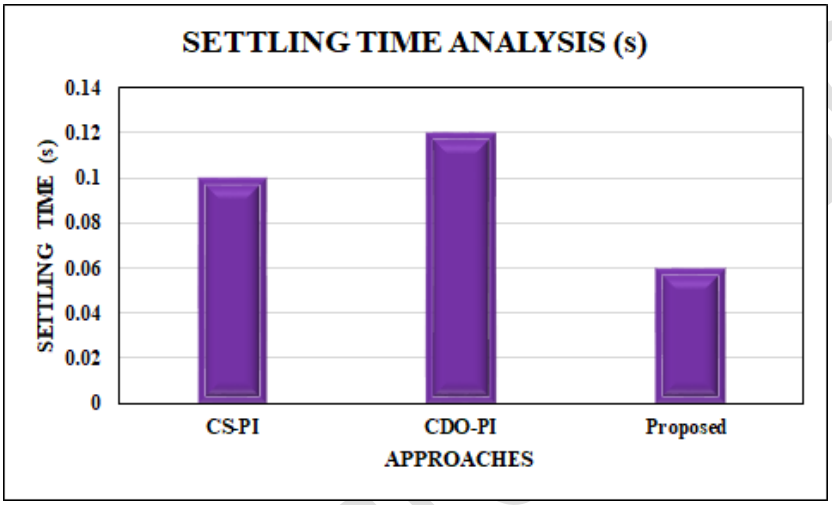


Fig. 21. Analysis of settling time

Fig. 21 displays the settling time analysis of PI control approaches. Owing to poorer control parameter optimisation and slower damping characteristics, the CDO-PI [24] controller has the slowest response at 0.12 s, while the CS-PI [22] controller has a greater settling time of 0.1 s. The developed control strategy, on the other hand, validates quicker convergence than both CS-PI and CDO-PI while preserving stable operation, attaining a better performance with a settling time of 0.06 s.

4. Conclusion

The PV-powered EV system for effective energy conversion and management is developed in this research. The QVLB converter maintains lower switching stress, improved efficiency and power transfer capabilities while attaining a high voltage conversion ratio. By automatically adjusting controller parameters to changes in irradiation and load demand, the integration of the BM-PI controller permits the regulation of the voltage.

Uncorrected Proof

Additionally, the battery storage system's bidirectional converter permits efficient charging and discharging processes, enhancing energy efficiency and preserving system stability under transitory circumstances. When compared to traditional control approaches, the developed controller exhibits quick dynamic response, lower steady-state error and superior voltage regulation. The outcomes of the simulation in MATLAB tool confirm that the converter and intelligent control are effective in producing dependable power conversion and enhanced motor driving characteristics with efficiency of 94.9 %. Thus, the developed system is a capable solution for EVs fuelled by renewable energy in the future owing its improved efficiency and stability. The performance of the QVLB converter and BMO-PI controller has not yet been verified using a hardware arrangement; instead, they are currently only evaluated using MATLAB simulations. Future research will concentrate on developing a small-scale hardware prototype that combines the BLDC motor drive, bidirectional battery interface, PV source and QVLB converter. To verify voltage gain, the reported efficiency, DC-link voltage regulation, and dynamic response, the prototype will be tested under various irradiance and load circumstances.

References

[1] M.T. Sarker, M. Al Qwaid, S.J. Shern, and G. Ramasamy, “AI-Driven optimization framework for smart EV charging systems integrated with solar PV and BESS in High-Density residential environments”, 2025 World Electric Vehicle Journal, vol. 16, no. 7, pp. 385.

[2] M. M. Enam, N. Ananthasaravanan, P. Kavitha, S. Rahini, B. Nilophine and D. Karthikeyan, “Design and Development of Coupled Inductor Interleaved Boost Converter for High Voltage EV Charging Applications,” 2026 9th International Conference on Circuit, Power & Computing Technologies (ICCPCT), Kollam, India, 2026, pp. 1362-1367.

[3] D. Karthikeyan, P. Kavitha, R. Sundar, M. Gopalswamy, C. Fabbina and T. S. Ganesh, “Efficient Power Conversion for EV Swapping Station Using High Gain KY Converter and Optimized MPPT Control,”

Uncorrected Proof

2025 IEEE International Conference on Emerging Trends in Computing and Communication (ETCOM), Mangalore, India, 2025, pp. 1-7.

[4] M. S. Thanaraj, R. Poomalai, R. Vibin, V. Kamalakar, S. Gupta, M. P. R. Perumal, and M. Vadivel, "Sustainable Energy Integration for Seawater Desalination", 2024 In Journal of Environmental Protection and Ecology, vol. 25, no. 6, pp. 2086–2096.

[5] B. N. Kommula, T. Thangam, P. K Gouda, K. S. Kavin, S. Tamil Selvi, N. V. Uma Reddy, "Solar-Powered Electric Vehicles: High-Gain SEPIC Converter with Neural Network MPPT". In International Conference on Power Electronics and Renewable Energy Systems, pp. 337-348. 2024. Singapore: Springer Nature Singapore.

[6] S. Smonia Joe Princy, C. Hentry, N. Alharbi, H. Siddiq, M. Refaei, H. Alzahrani, M.R. Bindhu, V. Sarojini, and S. Sasi Florence, "Synergistic Antimicrobial and Photocatalytic Properties of PVP-Ag-PEG Nanocomposites for Sustainable Leachate Treatment", 2024 Journal of Inorganic and Organometallic Polymers and Materials, pp. 1-19.

[7] A. Karthick, "Review on State of charge prediction of battery management system in electric vehicles", 2025 Proceedings of the Institution of Mechanical Engineers, Part D: Journal of Automobile Engineering, pp. 09544070251380931

[8] K. Dhineshkumar, M. Deepak, R. Mythili and S. Kumari, "Investigation of Dual Active Bridge Converters for Electric Vehicle Battery Charger. In 2025 International Conference on Sustainable Technology in Energy and Power Systems (STEPCon), pp. 215-220, 2025, IEEE.

[9] V. Sakthimurugan, Y. Devarajan, and R. P. Singh, (2025). "Advancing Electric Vehicles through Nanotechnology: Overcoming Challenges in Battery Performance, Energy Efficiency, and Sustainability", 2025 Battery Energy, vol. 5, no. 1.

Uncorrected Proof

[10] P. Das, S. Gope, D. Das, R. Chakraborty, and P. Das, "Optimal allocation of EV charging stations in a PV and wind energy sources integrated distributed system", 2025 Electrical Engineering, vol. 107, no. 9, pp. 12669-12683.

[11] Y.B. Koca, "Adaptive energy management with machine learning in hybrid PV-wind systems for electric vehicle charging stations", 2025 Electrical Engineering, vol. 107, no. 4, pp. 4771-4782.

[12] B. Shanmugam, "Hydrogen-centric multi-energy systems for high-renewables grids: Technologies, flexibility services, and deployment pathways-A critical review", 2026 International Journal of Hydrogen Energy, vol. 223, pp. 154429

[13] S. Ahmed, A. Ali, S.A. Qadir, D. Ramunno, and A. D'Angola, "Modelling of energy management strategies in a PV-based renewable energy community with electric vehicles", 2025 World Electric Vehicle Journal, vol. 16, no. 6, pp. 302.

[14] S. V. K. Naresh and S. Peddapati, "New family of transformer-less quadratic buck-boost converters with wide conversion ratio", 2021 Int. Trans. Electr. Energy Syst., vol. 31, no. 11, pp. 1–21.

[15] S. Naresh, S. Peddapati and M. L. Alghaythi, "Non-Isolated High Gain Quadratic Boost Converter Based on Inductor's Asymmetric Input Voltage", 2021 IEEE Access, vol. 9, pp. 162108-162121.

[16] S. Gopinathan, V. S. Rao and S. K, "Controllability Analysis and Controller Design of Higher Order Novel Switched Inductor-Capacitor DC-DC Converters", 2023 IEEE Trans. Ind. Electron., early access.

[17] B. Krishna and V. Karthikeyan, "Active Switched-Inductor Network Step-Up DC–DC Converter with Wide Range of Voltage-Gain at the Lower Range of Duty Cycles", 2021 IEEE J. Emerg. Sel. Topics Ind. Electron, vol. 2, no. 4, pp. 431-441.

Uncorrected Proof

[18] S. Gopinathan, V. S. Rao and K. Sundaramoorthy, “Family of NonIsolated Quadratic High Gain DC–DC Converters Based on Extended Capacitor-Diode Network for Renewable Energy Source Integration”, 2022 IEEE J. Emerg. Sel. Topics Power Electron, vol. 10, no. 5, pp. 6218- 6230.

[19] A. S. Mansour, A. H. H., Amer, E. E. El-Kholy, and M. S. Zaky, “High gain DC/DC converter with continuous input current for renewable energy applications”, 2022 Sci. Reports., vol. 12, (1), 12138. (2022).

[20] S. Ahmad, M. Nasir, J. Dąbrowski, and J. M. Guerrero, “Improved topology of high voltage gain DC–DC converter with boost stages”, 2021 Int. J. Electron. Lett., vol. 9, no. 3, pp. 342–354.

[21] Y. Akarne, A. Essadki, T. Nasser, M. Annoukoubi, and S. Charadi, “Optimized control of grid-connected photovoltaic systems: Robust PI controller based on sparrow search algorithm for smart microgrid application”, 2025 Global Energy Interconnection.

[22] Y.R. Sankar, and K.C. Sekhar, “Hybrid PV/fuel cell based system using integrated SEPIC-Cuk converter with crow search optimized PI controller”, 2024 Int. J. Power Electron. Drive Syst. (IJPEDS), vol. 15, no. 3, pp. 1726-1738.

[23] J.A. Glenn, and S. Alavandar, “Hybrid optimized PI controller design for grid tied PV based electric vehicle”, Intell Autom Soft Comput, vol. 36, no. 2, pp. 1523-1545.

[24] S. Shyma, R. Brinda, and L. Padmasuresh, “A High-Efficiency PV-Based EV Charging System with SEPIC-Cuk Converter and Energy Management”, e-Prime-Advances in Electrical Engineering, Electronics and Energy, pp. 101064.

Uncorrected Proof